

Heating and cooling by iron in cool star winds

P. Woitke and E. Sedlmayr

Institut für Astronomie und Astrophysik, TU Berlin, Sekr. PN 8-1, Hardenbergstrasse 36, D-10623 Berlin, Germany (woitke@physik.tu-berlin.de)

Received 22 December 1998 / Accepted 9 March 1999

Abstract. The role of iron for the energy balance in the extended atmospheres and circumstellar envelopes of cool stars is explored. Based on large non-LTE model atoms for Fe I and Fe II, we study the influence of fine-structure, forbidden, permitted and bound-free transitions on the radiative heating and cooling of the gas under various temperature, density and radiation field conditions. The results are compared to those obtained in LTE and to those calculated when ignoring optical depth effects in the lines. The number of levels in the model atoms necessary to achieve convergence of the results is discussed.

Key words: atomic processes – hydrodynamics – radiation mechanisms: thermal – shock waves – stars: chromospheres – stars: circumstellar matter

1. Introduction

Investigations on the thermal energy balance of gases can provide important scientific insight into various long-standing astrophysical problems, as for example the formation of chromospheres, the propagation of shock waves, and the generation of stellar winds.

The starting point of a thermodynamical description of the nebular-like gases in chromospheres and stellar winds is the determination of the important *radiative heating/cooling rates*, which are usually the leading terms in the energy equation. The iron group ions and especially the neutral iron atom have special properties concerning their possible efficiency as heating or cooling agents: 1) Iron possesses numerous electronic states at low excitation energies which can be easily (de-)excited by collisions. 2) Thousands of permitted, forbidden and fine-structure lines cause a strong coupling between the radiation field and the level populations. Lines of iron are visible in almost every astronomical object. 3) Iron is a fairly abundant element not much depleted by molecule formation. These facts alone immediately suggest that iron could be important for the energy balance of the gas.

Nevertheless, the role of iron as a contributor to the radiative heating and cooling in cool star winds has scarcely been investigated¹. Vernazza et al. (1981) computed radiative heating/cooling rates including a 15-level-atom plus continuum

¹ Possibly due to the complexity of the atom in conjunction with the general difficulties encountered in non-LTE investigations

for Fe I for the solar chromosphere based on a semi-empirical model, where the temperature structure is chosen to best match the observations. Hollenbach & McKee (1989) modelled J shocks² in molecular clouds including 15 fine-structure and forbidden Fe I and Fe II cooling lines.

Carpenter et al. (1997) observed and modelled Fe I and Fe II UV lines of the carbon star TX Psc which provided various informations about the properties of its outer atmosphere, as for example the velocity and ionisation structures, and the line formation mechanisms (thermal excited or fluorescent). Recently, Aoki et al. (1998) detected surprisingly strong emission in infrared fine-structure lines in both carbon-rich and oxygen-rich AGB stars. They found that the C-stars mainly show Fe I emission lines, whereas the M-stars apparently show mainly Fe II lines. An explanation for the strength of the lines in LTE was difficult to achieve, as the authors were forced to assume very high densities around these stars.

In this paper, we investigate the efficiency of radiative heating and cooling by Fe I and Fe II. We calculate the total heating/cooling rates under various density, temperature and radiation field conditions. The paper is organised as follows. In Sect. 2, the basic equations and assumptions are outlined. Sect. 3 describes the model atoms for Fe I and Fe II. Sect. 4 summarises the methods used for the computational solution of the statistical equations and describes how the calculations for iron are embedded in a larger steady-state non-LTE model of the gas. In Sect. 5, the results for various gas densities, temperatures and background radiation fields are presented and discussed. Sect. 6 contains some general remarks on the importance of the different types of spectral lines and includes some generalisations concerning other atoms. Our conclusions are outlined in Sect. 7.

2. Basic equations

An N -level-atom with continuum denoted by κ is considered. We assume that the characteristic time-scales of the atomic processes (excitation and ionisation) are short compared to those for changes in the ambient medium (both gas parameters and radi-

concerning “ultra-cool stellar atmospheres” (see e. g. discussion in Luttermoser & Johnson 1992).

² Shocks where the gas properties “jump” from their pre-shock to their post-shock values and where ambipolar diffusion is negligible.

tion field). In this case, the level populations n_i ($i = 1, \dots, N, \kappa$) can be calculated by means of the statistical equations

$$n_i \sum_{j \neq i} R_{ij} = \sum_{j \neq i} n_j R_{ji} \quad (1)$$

together with the auxiliary condition $n^{\text{tot}} = \sum_{i=1}^N n_i$. The rate coefficients R_{ij} describe the various physical processes taken into account, which are collisional (de-)excitation, line absorption, spontaneous and stimulated line emission, collisional ionisation and three-body-recombination, photo-ionisation and direct photo-recombination:

$$R_{ul} = A_{ul} P_{ul}^e (1 + j_{\nu_{ul}}) + C_{ul} \quad (2)$$

$$R_{lu} = \frac{g_u}{g_l} \left(A_{ul} P_{ul}^e j_{\nu_{ul}} + C_{ul} e^{-\frac{\Delta E_{ul}}{kT}} \right) \quad (3)$$

$$R_{l\kappa} = \frac{8\pi}{c^2} \int_{\nu_{\text{thr}}^l}^{\infty} j_{\nu} \sigma_l^{\text{bf}} \nu^2 d\nu + C_{l\kappa} \quad (4)$$

$$R_{\kappa l} = \frac{n_e}{S_l} \left(\frac{8\pi}{c^2} \int_{\nu_{\text{thr}}^l}^{\infty} (1 + j_{\nu}) e^{-\frac{h\nu}{kT}} \sigma_l^{\text{bf}} \nu^2 d\nu + C_{l\kappa} \right) \quad (5)$$

These formulations include the Milne-type relations between the respective forward and reverse rates (see Woitke et al. 1996). h , c and k are Planck's constant, the speed of light and Boltzmann's constant. T is the kinetic temperature and n_e the electron density. $\Delta E_{ul} = E_u - E_l$ is the energy difference between the upper (u) and lower (l) state with degeneracies g_u and g_l . ν is the frequency and ν_{ul} the line center frequency. A_{ul} is the Einstein coefficient for spontaneous emission. C_{ul} and $C_{l\kappa}$ are the rate coefficients for collisional de-excitation and collisional ionisation, respectively. $\sigma_l^{\text{bf}}(\nu)$ is the photo-ionisation cross section, $S_l(T)$ the Saha function and $\nu_{\text{thr}}^l = \chi_l/h$ the threshold frequency of level l . $\chi_l = \chi - E_l$ is the ionisation potential of level l .

In order to approximately account for optical depth effects in the lines, an escape probability method is used. The mean escape probabilities P_{ul}^e are calculated by applying Sobolev theory according to the mean velocity gradient $\langle \frac{dv}{dl} \rangle$ (see Woitke et al. 1996 for further details). The radiation field is thereby formally split into continuum plus lines and the local continuum (background) mean intensity is expressed in terms of the dimensionless quantity $j_{\nu} = J_{\nu}^{\text{cont}} c^2 / (2h\nu^3)$. The gas is assumed to be optically thin in the continuum, i. e. the background mean intensity J_{ν}^{cont} is used for the calculation of the bound-free radiative rates (Eqs. 4 and 5).

The radiative net heating rate is calculated after having solved the statistical equations. The net heating rate is defined as the total net gain of photon energy per time and volume. It can be split into the rates caused by the radiative bound-bound and bound-free transitions:

$$Q_{\text{rad}}^{\text{bb}} = \sum_{\text{lines}} \Delta E_{ul} A_{ul} P_{ul}^e \left(n_l \frac{g_u}{g_l} j_{\nu_{ul}} - n_u (1 + j_{\nu_{ul}}) \right) \quad (6)$$

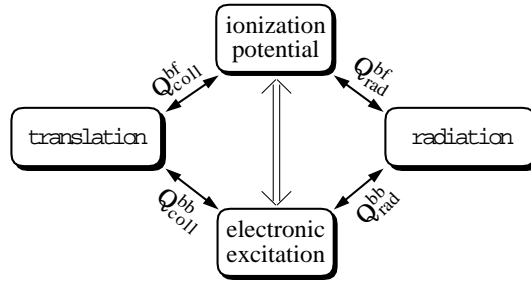


Fig. 1. Energy fluxes between the pools of thermal kinetic energy (“translation”), ionisation potential and electronic excitation energies, and radiation energy. Positive fluxes (“heating”) are directed to the left.

$$Q_{\text{rad}}^{\text{bf}} = \frac{8\pi h}{c^2} \sum_{\ell=1}^N \int_{\nu_{\text{thr}}^{\ell}}^{\infty} \left(n_{\ell} j_{\nu} - \frac{n_{\kappa} n_e}{S_{\ell}} (1 + j_{\nu}) e^{-\frac{h\nu}{kT}} \right) \nu^3 \sigma_{\ell}^{\text{bf}} d\nu \quad (7)$$

In order to study the role of the spectral lines of different strength, we define the following classes of spectral lines by

$$\text{fine-structure} : \text{inter-level transition} \quad (8)$$

$$\text{forbidden} : A_{ul} < 10^4 \text{ s}^{-1} \quad (9)$$

$$\text{permitted} : A_{ul} > 10^4 \text{ s}^{-1} \quad (10)$$

The heating/cooling rates of these classes are obtained by calculating Eq. (6) separately for all lines of the respective transition type

$$Q_{\text{rad}}^{\text{bb}} = Q_{\text{fine}}^{\text{bb}} + Q_{\text{forb}}^{\text{bb}} + Q_{\text{perm}}^{\text{bb}} \quad (11)$$

In statistical equilibrium, the energy contained in the atom in the form of electronic excitation and ionisation potential energy is constant. The atom only transmits energy from the radiative to the thermal kinetic pool of energy or vice versa, and the net heating rate is equal to the total net gain of thermal kinetic energy per time and volume (see Fig. 1). This rate can be split into the rates caused by (de-)exciting collisions and by the rates due to bound-free transitions

$$Q_{\text{coll}}^{\text{bb}} = \sum_{\ell=1}^{N-1} \sum_{u=\ell+1}^N C_{u\ell} \Delta E_{u\ell} \left(n_u - n_{\ell} \frac{g_u}{g_{\ell}} e^{-\frac{\Delta E_{u\ell}}{kT}} \right) \quad (12)$$

$$Q_{\text{coll}}^{\text{bf}} = Q_{\text{coll}}^{\text{bf}} - \sum_{\ell=1}^N \chi_{\ell} (n_{\ell} R_{l\kappa} - n_{\kappa} R_{\kappa l}) \quad (13)$$

$$Q_{\text{rad}}^{\text{bb}} + Q_{\text{rad}}^{\text{bf}} = Q_{\text{coll}}^{\text{bb}} + Q_{\text{coll}}^{\text{bf}} \quad (14)$$

Eq. (14) can be used to check the quality of the solution of the statistical equations.

3. Atomic data

3.1. Model atom for Fe I

The level energies E_{ℓ} , degeneracies g_{ℓ} and Einstein coefficients A_{ul} for the lowest 200 states (ordered by energy) of the neutral iron atom have been obtained from the NIST³ (Fuhr et al. 1988)

³ <http://aeldata.nist.gov/archive/holdp.html>

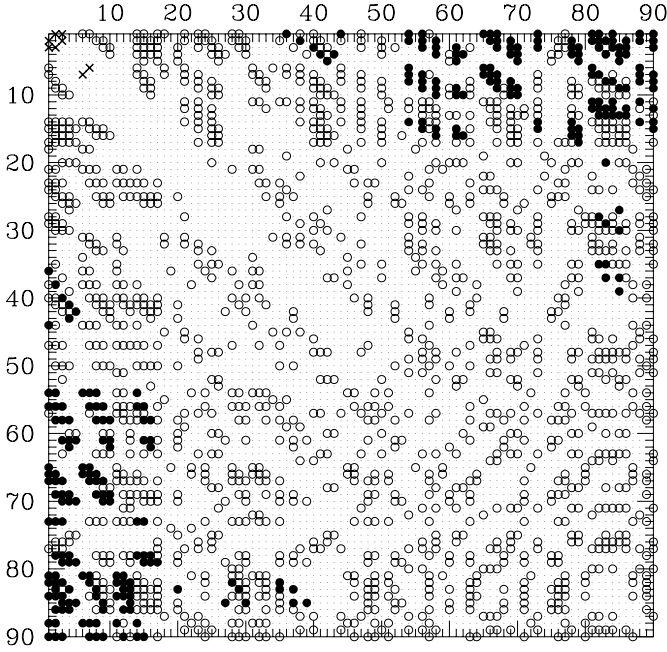


Fig. 2. Types of radiative transitions between the lowest 90 states (ordered by energy) of Fe I (cross: fine-structure, open circle: forbidden, full circle: permitted, dot: no radiative transition). The higher levels 91–200 are not depicted.

and from KURUCZ’s database⁴ (Kurucz 1988). Both databases agree with each other concerning the electronic configurations and the energies of these levels. However, the Einstein coefficients may differ substantially. KURUCZ’s list includes many more lines (especially forbidden transitions) for highly excited states, whereas the NIST database has more data for lines among low levels. We have taken KURUCZ’s line-list as the starting point and have added/replaced all Einstein coefficients listed by NIST with $A_{ul} > 0$. Four fine-structure lines (2-1, 3-1, 3-2, 7-6) have also been included with Einstein coefficients taken from Hollenbach & McKee (1989).

Fig. 2 gives an impression of the complexity of the radiative line data for Fe I. According to our working definition Eqs. (8) to (10), there are 4 fine-structure, 2420 forbidden and 1289 permitted lines in the Fe I model atom covering wavelengths between 2140 Å and 89 μm. Note that in order to account for the first (semi-)permitted line (4375.9 Å) the model atom has to include at least 36 levels (the z^7F^0 -level located at 22845.9 cm⁻¹ ≈ 2.8 eV).

An ionisation potential of $\chi = 63737 \text{ cm}^{-1} \approx 7.87 \text{ eV}$ is assumed and the partition function of Fe II is chosen to be 30. The photo-ionisation cross sections are assumed to vary with frequency as

$$\sigma_{\ell}^{\text{bf}}(\nu) = \sigma_{\ell}^0 \left(\frac{\nu_{\text{thr}}^{\ell}}{\nu} \right)^3. \quad (15)$$

The threshold cross sections σ_{ℓ}^0 are adopted from (Vernazza et al. 1981) for the levels listed therein and is assumed to be equal

to $3.3 \cdot 10^{-18} \text{ cm}^2$ for all other levels. The latter is chosen such that the total direct recombination rate

$$\alpha(T) = \sum_{\ell=1}^N \frac{8\pi}{c^2 S_{\ell}} \int_{\nu_{\text{thr}}^{\ell}}^{\infty} e^{-\frac{h\nu}{kT}} \sigma_{\ell}^{\text{bf}} \nu^2 d\nu \quad (16)$$

equals $1.4 \cdot 10^{-13} \text{ cm}^3 \text{ s}^{-1}$ at 10000 K, which agrees with the known rate (Landini & Fossi 1990). The rates of collisional de-excitation and collisional ionisation are calculated according to

$$C_{ul}(T) = n_e \gamma_{ul}^e(T) + n_h \gamma_{ul}^h(T) \quad (17)$$

$$C_{\ell\kappa}(T) = n_e \beta_{\ell}^e(T) + n_h \beta_{\ell}^h(T) \quad (18)$$

where γ^e , γ^h and β^e , β^h denote the rate coefficients for electron and heavy particle impact, respectively. The heavy particle density is approximated by $n_h = n_{\langle\text{H}\rangle} + n_{\langle\text{He}\rangle}$, where $n_{\langle\text{H}\rangle}$ and $n_{\langle\text{He}\rangle}$ are the total number densities of hydrogen and helium nuclei. Collisional de-excitation rates for both electron and heavy particle impact for transitions among lower levels have been summarised by Hollenbach & McKee (1989) for neutral and singly ionised atoms including Fe I. We have adopted their rates for the transitions 2-1, 3-1, 3-2, 6-1, 7-1, 7-6 and have completed the missing rates among the 10 lowest levels ($a^5D_4, \dots, a^5D_0, a^5F_5, \dots, a^5F_1$) by assuming $g_{\ell} \gamma_{ul}^e = g_{\ell'} \gamma_{ul}$ and $\gamma_{u'\ell} = \gamma_{ul}$ with respect to the nearest given rate. Electron collision rates for transitions which have a permitted radiative counterpart are calculated according to the van Regemorter-formula (van Regemorter 1962). For all other transitions we assume a constant collision strength of $\Upsilon_{ul} = 0.1 \sqrt{T/10000\text{K}}$ which is related to the de-excitation rate coefficient by

$$\gamma_{ul}^e(T) = \frac{8.63 \cdot 10^{-6} \Upsilon_{ul}(T)}{g_u \sqrt{T}}. \quad (19)$$

All missing heavy particle collision rate coefficients γ_{ul}^h are assumed to be $10^{-12} \text{ cm}^3 \text{ s}^{-1}$.

The collisional ionisation rates are calculated from

$$\beta_{\ell}^e(T) = \frac{A_{\text{col}} \sqrt{T} Z}{\sum_{\ell=1}^N g_{\ell}} \left(1 + \frac{0.1 T}{T_{\text{col}}} \right) e^{-\frac{T_{\text{col}} - E_{\ell}/k}{T}} \quad (20)$$

Eq. (20) yields the correct total collisional ionisation rate by electron impact $\sum n_{\ell} \beta_{\ell}^e$ in LTE as published by Landini & Fossi (1990). Parameters are $T_{\text{col}} = 91300 \text{ K}$ and $A_{\text{col}} = 1.26 \cdot 10^{-10} \text{ cm}^2$. $Z = \sum_{\ell=1}^N g_{\ell} \exp(-E_{\ell}/kT)$ is the partition function. The collisional ionisation rates for heavy particle impact $\beta_{\ell}^h(T)$ are assumed to be $1.7 \cdot 10^{-4}$ times the electron rates as is true for hydrogen (Drawin 1969).

3.2. Model atom for Fe II

The positive iron atom is modelled without continuum since the high ionisation potential of 16.16 eV is assumed to prevent considerable ionisation of Fe II in the investigated parameter regime of this paper. The total particle density of Fe II atoms is assumed to be given by n_{κ} from the solution of the statistical equations for Fe I.

⁴ <http://cfa-www.harvard.edu/amp/data/kur23/sekur.html>

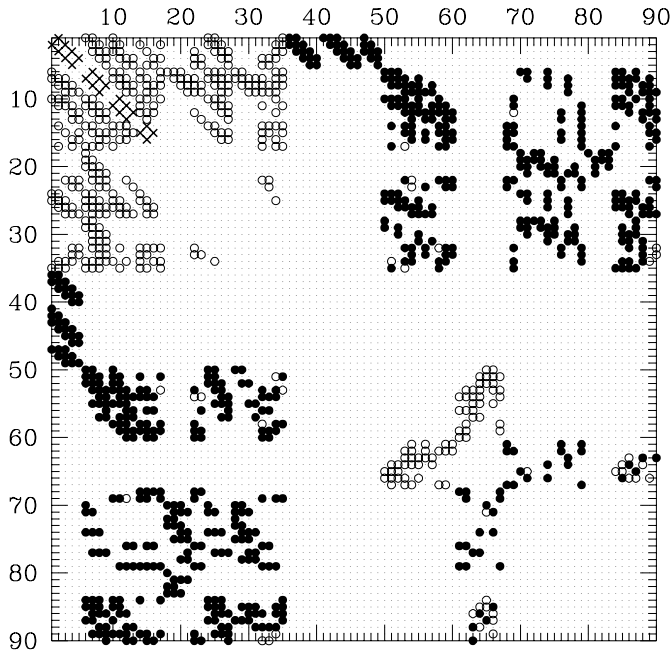


Fig. 3. Types of radiative transitions within the lowest 90 states (ordered by energy) of Fe II (cross: fine-structure, open circle: forbidden, full circle: permitted, dot: no radiative transition). The higher levels 91–142 (not depicted) mainly possess permitted radiative transitions.

Extensive atomic data (radiative + collisional) for many astrophysically interesting positive ions have recently been published in the CHIANTI database (Dere et al. 1997). Besides the level energies, degeneracies, transition wavelengths and Einstein coefficients, these data include electron collision rates according to a 5-parameter fit as a function of temperature (Burgess & Tully 1992), which provides an excellent base for non-LTE investigations in a wide temperature range.

The Fe II CHIANTI data set comprises 142 levels with energies up to 93487.6 cm^{-1} ($\approx 11.6 \text{ eV}$), 1268 radiative transitions (1098 \AA to $87.3 \mu\text{m}$) and collision rates for transitions from all levels down to the lowest 35 levels. We have completed the missing collision rates by the van Regemorter–formula (van Regemorter 1962) for permitted transitions and by assuming a constant collision strength of $\Upsilon_{ul} = 0.1$ otherwise. All heavy particle collision rate coefficients γ_{ul}^h are assumed to be $10^{-12} \text{ cm}^3 \text{ s}^{-1}$.

We find 12 fine-structure, 246 forbidden and 1010 permitted transitions in the database (see Fig. 3). In order to catch the first permitted lines (2600.2 and 2626.5 \AA) the Fe II model atom must include the 36^{th} level z^6D^0 (located at $38450.0 \text{ cm}^{-1} \approx 4.8 \text{ eV}$).

4. Calculation of the composition of the gas

A consistent non-LTE modelling of Fe I and Fe II cannot be performed on its own, but must be part of a larger model which includes the determination of the Fe I/Fe II ratio and especially the electron density, which enters into the calculation of the collision rates.

Table 1. Overview of model atoms

atom	N	E_N [eV] ($\frac{E_N}{\chi}$)	no. of lines*	references
H	5	13.1 (96%)	0 + 0 + 10	2,3
He I	5	21.1 (86%)	0 + 5 + 3	1,2
He II	25	52.2 (96%)	0 + 1 + 72	4
C I	11	9.2 (82%)	3 + 10 + 12	1,3,6,8
C II	20	21.0 (86%)	1 + 5 + 37	4
N I	28	12.5 (86%)	1 + 29 + 67	1,5,6,7
N II	23	20.7 (70%)	2 + 16 + 68	4
O I	29	12.4 (91%)	3 + 7 + 56	1,5,6
O II	15	26.3 (75%)	1 + 8 + 29	4
Ne I	1	0.0 (0%)	0 + 0 + 0	1
Ne II	3	26.6 (65%)	1 + 0 + 2	4
Na I	20	4.6 (89%)	0 + 4 + 56	1,5
Mg I	29	6.8 (89%)	3 + 18 + 82	1,5,7
Mg II	21	12.9 (86%)	0 + 0 + 34	4
Al I	30	5.6 (94%)	0 + 21 + 113	1,5
Si I	30	6.6 (78%)	3 + 32 + 98	1,5,6
Si II	15	10.5 (64%)	1 + 10 + 24	4
S I	30	9.0 (87%)	3 + 4 + 79	1,5,6
S II	28	14.9 (64%)	2 + 30 + 66	4
Ca I	29	4.8 (78%)	0 + 64 + 74	1,5
Ca II	5	3.3 (27%)	0 + 2 + 5	8
Fe I	200	5.8 (74%)	4 + 2420 + 1289	see text
Fe II	142	11.6 (72%)	12 + 246 + 1010	see text

* fine-structure + forbidden + permitted

(1) OPACITY PROJECT (Seaton et al. 1994) with corrected threshold wavelengths (see text)

(2) Luttermoser & Johnson (1992)

(3) Vernazza et al. (1981)

(4) CHIANTI database (Dere et al. 1997)

(5) KURUCZ’s line-list (Kurucz 1988)

(6) Hollenbach & McKee (1989)

(7) Mendoza (1983)

(8) R. Sutherland (1997, priv. comm.)

We consider a mixture of the elements H, He, C, N, O, Ne, Na, Mg, Al, Si, S, Ca, and Fe with solar abundances according to Anders & Grevesse (1989, “Photosphere”-column). The neutral atoms are modelled with continuum, the ions without continuum. Table 1 summarises the references for the respective model atoms. The line data have been taken mainly from the KURUCZ and the CHIANTI databases. The collisional de-excitation rates for neutral atoms are calculated similarly as stated in Sect. 3.1. The collisional rates for ions are adopted from the CHIANTI database. Photo-ionisation cross sections for all states of all atoms other than H I and Fe I have been obtained from the OPACITY PROJECT⁵ (Seaton et al. 1994) and smoothed to a 10 \AA -wavelength grid. We noticed that the OP threshold wavelengths are not very accurate (usually too short) and have scaled the cross sections as a function of wavelength according to the threshold wavelengths derived from the level energies and the ground state ionisation potentials (Allen 1973). Collisional ionisation rates are calculated according to Eq. (20) with the parameters A_{col} and T_{col} given by Landini & Fossi (1990).

⁵ <http://vizier.u-strasbg.fr/OP.html>

To summarise, the model atoms for species other than Fe I and Fe II contain between 5 and 30 levels, usually covering all known states with excitation energies lower than ~ 9 eV or (in case of Na I, Mg I, Al I and Si I) at least all states with excitation energies $\leq 78\%$ of the ionisation potential (exceptions: Ne I, Ne II, Ca II). The model atoms include all fine-structure and forbidden cooling lines, and collision rates listed by Hollenbach & McKee (1989), as well as the highly excited states with a considerable number of permitted transitions.

The concentration of 96 neutral diatomic and polyatomic molecules are calculated with respect to the total neutral atom densities by assuming chemical equilibrium. The electron density n_e and the total neutral atom densities n_{tot} are found by a Newton-Raphson iteration involving all elements under consideration in order to achieve the conditions of charge and particle conservation, respectively.

For practical reasons, it was not possible to use the full model atoms as described in Table 1 during the Newton-Raphson iteration. We have instead used truncated model atoms during this iteration (5-level-atoms for H, He I and C I, 3-level-atom for Na, 1-level-atom for all other atoms) which preliminarily determines the electron, ion, atom and molecule densities. In a second step, the full neutral atom models are calculated, and the atom and ion densities are corrected accordingly. In a third step, the ion model atoms are calculated.

According to the assumptions outlined, all results of the model calculations (including the Fe I and Fe II heating/cooling rates) depend on the following local parameters: $n_{\langle\text{H}\rangle}$, T , J_ν^{cont} and $\langle\frac{dv}{dl}\rangle$. The total hydrogen particle $n_{\langle\text{H}\rangle}$ is proportional to the mass density $\rho = n_{\langle\text{H}\rangle} \sum_{\text{El}} \epsilon_{\text{El}} m_{\text{El}}$ ($\log \rho \approx \log n_{\langle\text{H}\rangle} - 23.6$), where m_{El} and ϵ_{El} are the mass and the abundance of element El with respect to hydrogen.

5. Results

5.1. Investigated range of parameters

Density and temperature: The hydrogen particle density $n_{\langle\text{H}\rangle}$ and the kinetic temperature of the gas T are varied within the intervals $n_{\langle\text{H}\rangle} = 10^4 \dots 10^{14} \text{ cm}^{-3}$ and $T_g = 500 \dots 20000 \text{ K}$, respectively. The chosen ranges should cover most of the conditions present in the outer atmospheres, the chromospheres, and the inner parts of the circumstellar envelopes of both non-pulsating as well as pulsating stars, where shock waves can heat up the gas considerably.

Continuous background radiation field: The gas is assumed to be optically thin in the continuum and to be exposed to diluted star light, which is regarded as the typical situation for the gas in stellar winds. For the general purpose of this paper, we will consider a diluted Planckian background radiation field

$$J_\nu^{\text{cont}} = W_{\text{dil}} B_\nu(T_{\text{rad}}) \quad , \quad (21)$$

which roughly describes the spectral radiative energy distribution close to a stellar surface. B_ν is the Planck function, T_{rad} a radiation temperature and W_{dil} a dilution factor. The latter may

be identified with the fraction of the solid angle occupied by the stellar disk with radius R_* at radial distance r

$$W_{\text{dil}}(r) = \frac{1}{2} \left(1 - \sqrt{1 - R_*^2/r^2} \right) \quad . \quad (22)$$

In this case, $T_{\text{rad}} \approx T_*$ where T_* is the stellar temperature. If continuum optical depths effects are important in the circumstellar envelope, T_{rad} is usually smaller than T_* and W_{dil} is larger than predicted by Eq. (22), but Eq. (21) still provides a reasonable fit. We consider radiation temperatures between 0 and 5000 K in this paper.

For reasons of comprehensiveness, we will focus our interest in the present paper on a particular radial zone around $r/R_* = 2$ ($W = 0.067$). This region has proven to be important for the generation and the acceleration of cool star winds in many publications (e. g. Bowen 1988, Fleischer et al. 1992, Linsky et al. 1998). The depicted results are, however, similar to those obtained with other choices for r .

Velocity gradient: In spherical symmetry, the mean velocity gradient $\langle\frac{dv}{dl}\rangle$, which enters into the determination of the escape probabilities, can be expressed in terms of $|\frac{v}{r}|$ and $|\frac{\partial v}{\partial r}|$ (Woitke et al. 1996). Characteristic values in stationary stellar winds are $x v_\infty/R_*$ where x is of the order of unity at the sonic point and decreases to ~ 0.0067 at $100 R_*$. In the shocked atmospheres and envelopes of pulsating stars, the velocity gradients are much larger, roughly $v_1/(3\Delta r)$, where v_1 is the velocity of a nearby shock wave and Δr is a typical distance between the shock waves. We will mostly consider a value of $\langle\frac{dv}{dl}\rangle = 1 \text{ km s}^{-1}/50 R_\odot$, which is a typical value found in models for long-period variables (e. g. Fleischer et al. 1992). The influence of this parameter is discussed in Sect. 5.5.

5.2. Results as function of $n_{\langle\text{H}\rangle}$, T , and T_{rad}

Figs. 4, 5 and 6 show the resulting concentrations and heating/cooling rates of Fe I and Fe II in the (temperature/density)-plane for three different choices of the background radiation field.

1) For negligible continuous radiation fields (Fig. 4), iron is found to be predominately neutral up to temperatures of about 9000 K, triggered by the balance of collisional ionisation and photo-recombination. Since the rates of both processes scale linearly with n_e , fractional ionisation $n_{\text{Fe II}}/n_{\text{Fe I}}$ is mainly a function of temperature which results in essentially horizontal contour lines in the upper row of plots in the figure. The maximum possible concentration of Fe I or Fe II is $\log(\epsilon_{\text{Fe}}/\epsilon_{\text{H}}) = -4.33$. The degree of ionisation of the gas $n_e/n_{\langle\text{H}\rangle}$ (middle plot, upper row) shows a similar behaviour: The gas is found to be almost completely neutral below about 3000 K and about fully ionised beyond 10000 K. In comparison to LTE, the fractional ionisation of the gas is always lower, because the rates of photo-ionisation are zero, but the rates of photo-recombination are non-zero. At high densities and very low temperatures, iron is mainly present as $\text{Fe}(\text{OH})_2$ according to the model.

According to these results, the radiative cooling by iron in the case without background radiation field is dominated by Fe I

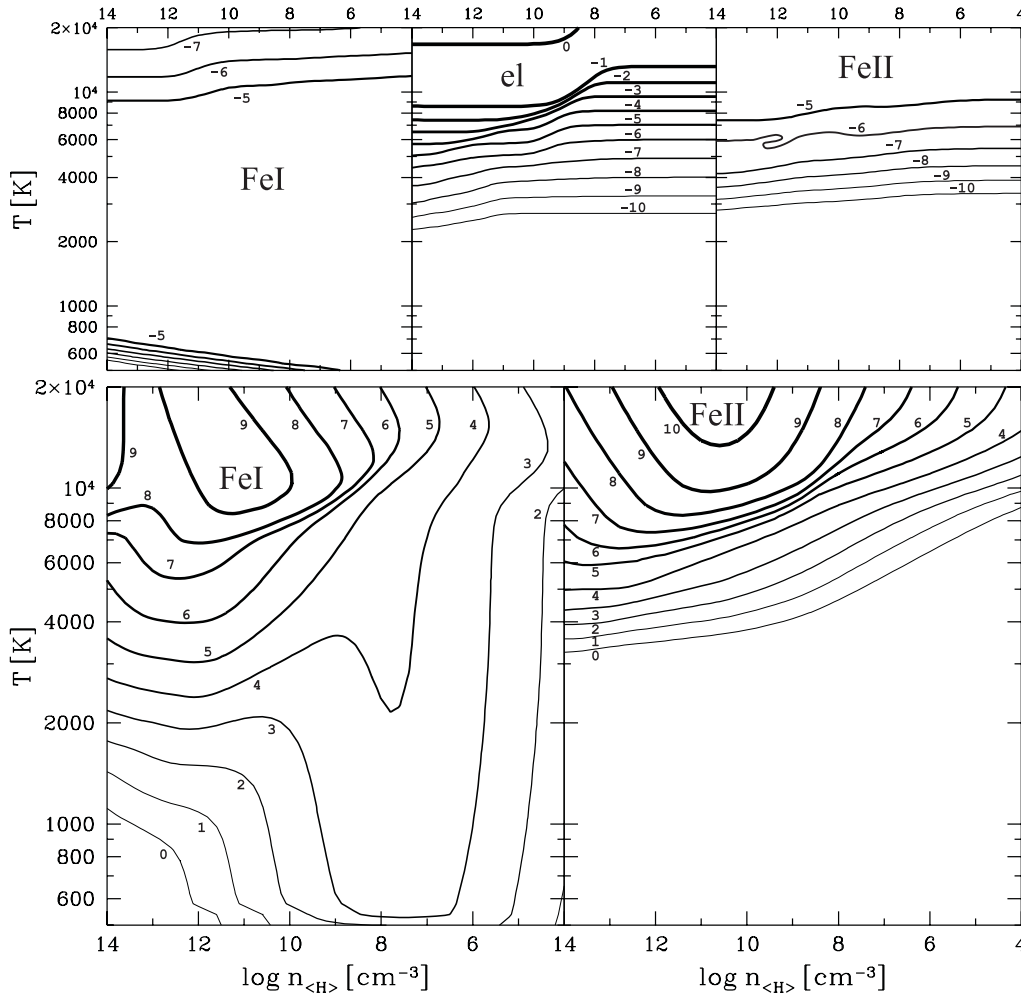


Fig. 4. Contour plots of the results *without background radiation field* as function of total hydrogen density $n_{(H)}$ and temperature T . The *upper* row of three contour plots shows the logarithmic concentrations of Fe I, electrons, and Fe II, respectively, with respect to hydrogen, e. g. $\log(n_{\text{Fe I}}/n_{(H)})$. The *lower* two contour plots depict the cooling rates per unit mass of the gas caused by Fe I and Fe II, respectively, e. g. $\log(-Q(\text{Fe I})/\rho) [\text{erg g}^{-1} \text{s}^{-1}]$. The small numbers indicate the values of the contour lines. Additional parameter: $\langle \frac{dv}{dt} \rangle = 1 \text{ km s}^{-1}/50 R_{\odot}$.

up to temperatures of about 9000 K (see lower row of plots in Fig. 4). The magnitude of the cooling rate is remarkable: For example, at $\log n_{(H)} = 10$ and $T = 6000 \text{ K}$ we find a cooling rate of $Q(\text{Fe I})/\rho \approx -8.3 \cdot 10^5 \text{ erg g}^{-1} \text{ s}^{-1}$, which translates to a rate of temperature decrease of $\frac{\partial T}{\partial t} |_{\rho=\text{const}} \approx -740 \text{ K/day}$ due to Fe I-cooling alone.

The depicted dependency of $Q_{\text{rad}}(\text{Fe I})/\rho [\text{erg/g/s}]$ on temperature and density is complex. At large densities ($\log n_{(H)} \gtrsim 11$) and temperatures 1000 K ... 4000 K, we find approximately horizontal contour lines for $Q_{\text{rad}}(\text{Fe I})/\rho$, which means that the iron cooling rates per mass are roughly density-independent in this regime: $\log(Q_{\text{rad}}(\text{Fe I})/\rho) \approx \text{const} + 8 \log(T)$, which is a typical LTE-feature (see Sect. 5.3). At small densities, however, the contour lines are roughly vertical: $Q_{\text{rad}}(\text{Fe I}) \approx f(T)\rho^2$. The reason for this behaviour is the insufficient collisional energy supply for the emitting states, which linearly reduces the cooling rates per mass with decreasing density (see Sect 6). The iron cooling is found to have a maximum efficiency around $\log n_{(H)} \approx 11 \dots 12$ at high temperatures, but around $\log n_{(H)} \approx 7 \dots 8$ at low temperatures, which indicates that different types of lines are responsible for the cooling at different temperatures. Consequently, neither $Q_{\text{rad}} \approx f(T)\rho^2$, nor $Q_{\text{rad}} = f(T)n_{\text{Fe I}}n_e$,

nor some other simple formula provides a reasonable approximation in the whole (temperature/density)-plane.

2) Fig. 5 shows the results for a diluted 3000 K-background radiation field. The concentrations are quite different from the case discussed before. Only at large densities $\log n_{(H)} \gtrsim 11$ and low temperatures $T \lesssim 4000 \text{ K}$, iron is still predominantly neutral. In the remaining part of the (temperature/density)-plane, iron is present mainly in form of Fe II. Accordingly, the electron concentration is much higher as compared to the case without continuous background radiation. A minimum electron concentration of about 10^{-6} to 10^{-4} is preserved even at very low temperatures due to photo-ionisation of metal atoms like Ca, Mg, Al, Si and Fe, depending on the density.

The cooling rates at high temperatures ($T \gtrsim 8000 \text{ K}$) are similar to those depicted in the previous figure, indicating that the background radiation only slightly disturbs the main energy fluxes between the various iron levels at high temperatures. According to its higher concentration, Fe II is the main coolant in most parts of the (temperature/density)-plane. Its maximum cooling efficiency is located around $\log n_{(H)} \approx 10 \dots 11$ at high temperatures, and around $\log n_{(H)} \approx 8 \dots 9$ at low temperatures. Due to the background radiation, now both Fe I and Fe II cause *radiative heating* at low temperatures (see dashed contour lines).

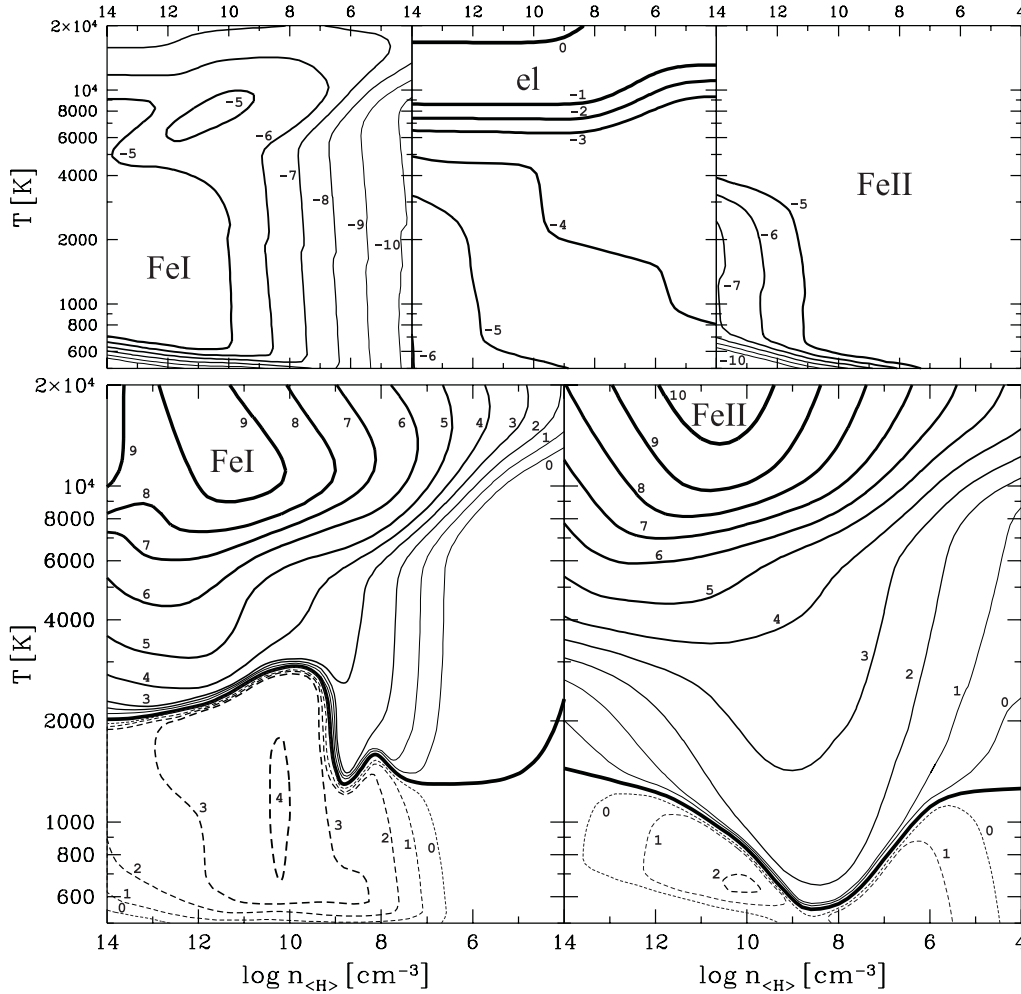


Fig. 5. Same as Fig. 4, but including a background radiation field with radiation temperature $T_{\text{rad}} = 3000$ K and radial distance r/R_* = 2. The thick full line in the lower two diagram indicates $Q = 0$. Underneath this line, the dashed contour lines indicate radiative heating rates, e. g. $\log(+Q(\text{Fe I})/\rho)$ [$\text{erg g}^{-1} \text{s}^{-1}$].

The complicated slope of the ($Q = 0$)-lines (thick full lines in the lower plots) are difficult to understand. Apparently, some especially efficient heating by forbidden Fe I-lines⁶ takes place at $\log n_{(\text{H})} \approx 10$, whereas for Fe II, some especially strong fine-structure cooling around $\log n_{(\text{H})} \approx 8 \dots 9$ is active⁷. In any case, the heating/cooling by Fe I and Fe II will drive the gas towards the respective ($Q = 0$)-line.

3) Fig. 6 shows the results for a diluted 5000 K-blackbody radiation field. The Fe II and electron concentrations are again higher when compared to the previous cases. Fe I can only exist (in considerable amounts) under high density conditions. This result is rather independent from the gas temperature, which indicates that collisional ionisation and three-body recombination are unimportant, unless the temperature exceeds 15000 K where the results are in fact similar to the cases discussed before.

The Fe II heating/cooling rate, which mostly dominates over Fe I, shows an interesting shift with respect to density between

⁶ Most efficient in this case are the Fe I a^5D-z^7D forbidden transitions having Sobolev optical depths between $10^0 \dots 10^3$ at wavelengths 5060–5250 Å.

⁷ Most efficient in this case are the Fe II a^6D-d^6D fine-structure transitions at $26 \mu\text{m}$ and at $35.3 \mu\text{m}$ having Sobolev optical depths around 10^{-1} .

maximum cooling (at $\log n_{(\text{H})} \approx 11$, solid lines) and maximum heating (at $\log n_{(\text{H})} \approx 8$, dashed lines), once more suggesting that different types of lines are responsible for the heating (at low T) and the cooling (at high T), respectively. Furthermore, regarding the depicted contour lines of $Q(\text{Fe I})$ in Fig. 6, the cooling decreases faster than the heating with decreasing density. Concerning Fe II, the heating rate only varies by 2-3 orders of magnitude, whereas the cooling rate varies by ~ 6 orders of magnitude. Consequently, the temperature where heating and cooling balance each other $T(Q = 0)$ is density-dependent and has its lowest value at high densities for both Fe I and Fe II (disregarding densities $\log n_{(\text{H})} < 6$), where the cooling is strongest. This general behaviour is also found for the other atomic heating/cooling rates (see Table 1).

5.3. Comparison with limiting cases

For hydrodynamical calculations it is important to know where certain limiting cases can be applied in order to minimise the numerical efforts for the proper calculation of the energy exchange rates between matter and the radiation field. It is very convenient, for example, to use the LTE approximation

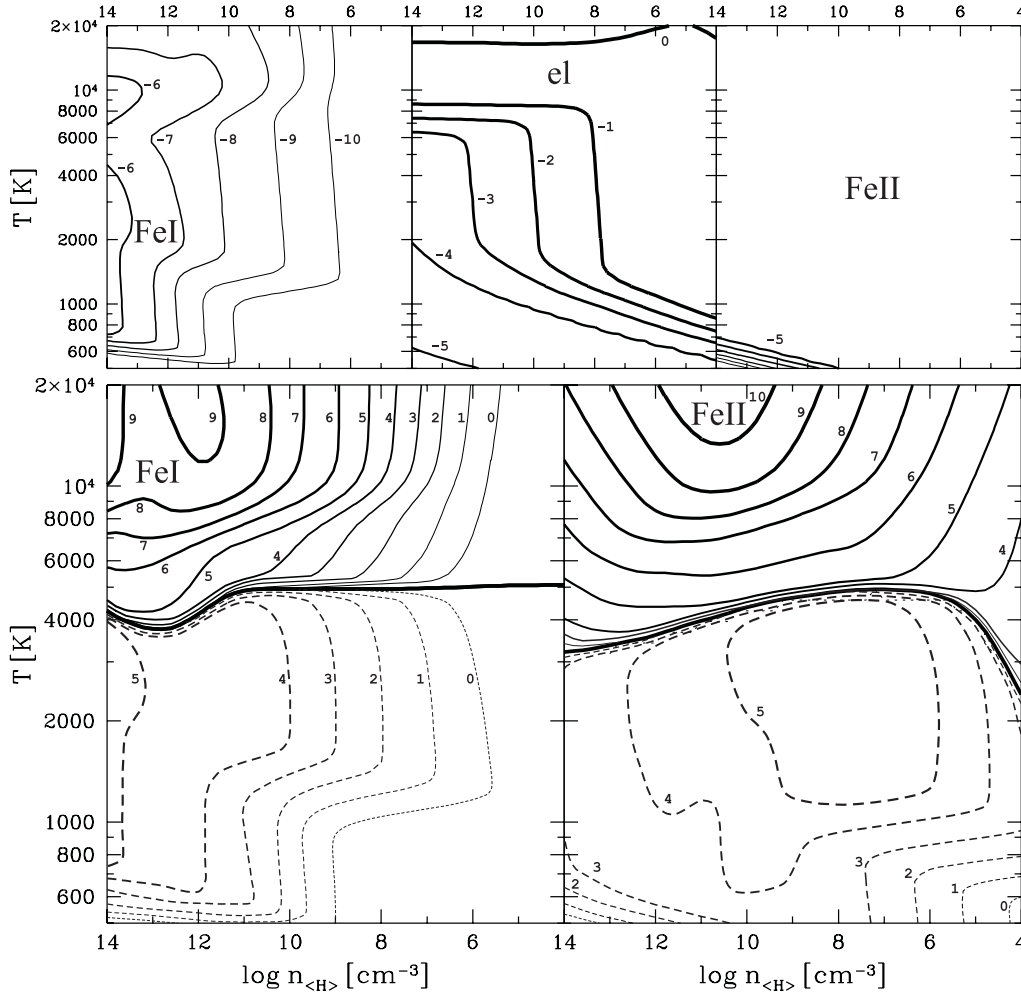


Fig. 6. Same as Fig. 4, but including a background radiation field with $T_{\text{rad}} = 5000$ K and radial distance $r/R_* = 2$.

$$Q_{\text{rad}}^{\text{LTE}} = 4\pi \int \kappa_{\nu} (J_{\nu} - B_{\nu}) d\nu, \quad (23)$$

where J_{ν} is the local mean intensity and B_{ν} the Planck function. κ_{ν} , in principle, is the full frequency-dependent true absorption coefficient which includes all lines, free-free and bound-free continua of the gas, but no scattering. It is difficult, though, to use Eq. (23) directly, because often (i) only a grey radiative transfer can be performed and detailed knowledge of J_{ν} is not available, or (ii) only a static radiative transfer can be performed, which ignores the Doppler-shifts of the lines thereby introducing errors in the calculation of J_{ν} just around those wavelength-positions where κ_{ν} is strongest (at the wavelength positions of optically thick lines).

When only a grey radiative transfer is available, the usage of mean opacities $\bar{\kappa}$ (Rosseland or Planck means) is a common procedure

$$Q_{\text{rad}}^{\text{LTE}} \approx 4\pi \bar{\kappa} (J - B). \quad (24)$$

For instance, Fokin e. g. (1992) applied Rosseland means in the energy equation concerning various non-linear pulsation models for RR Lyrae, β and δ Cepheids, and RV Tauri stars. Gauger et al. (1993) used Rosseland means in the energy equation for models of long-period variables. Höfner et al. (1998)

used Planck means for dynamic model atmospheres of AGB stars.

Other authors prefer to use pre-calculated cooling laws, as for example Bowen (1988) and Cuntz (1990), where the assumption $Q_{\text{rad}} \propto \rho^2$ is often made. However, this assumption is only valid in the low-density limiting case (see Sect. 6), where the cooling rates are limited by the amount of energy transferred to the emitters via collisions. If extrapolated to larger densities, this approach ignores optical depths effects in the lines.

In order to study the applicability of these two limiting cases, we have recalculated the Fe I and Fe II heating/cooling rates with the following modifications:

- i) The LTE-heating/cooling rate Q_{LTE} is obtained by assuming a Boltzmann distribution within the bound levels. The escape probabilities are included.
- ii) The heating/cooling rate in the optically thin limit Q_{thin} is calculated by putting all $P_{ul}^e = 1$, obtaining a new solution of the statistical Eqs. (1) and calculating the radiative heating/cooling rates for this case.

In both cases, the electron density and the Fe I/Fe II ratio have been left unchanged.

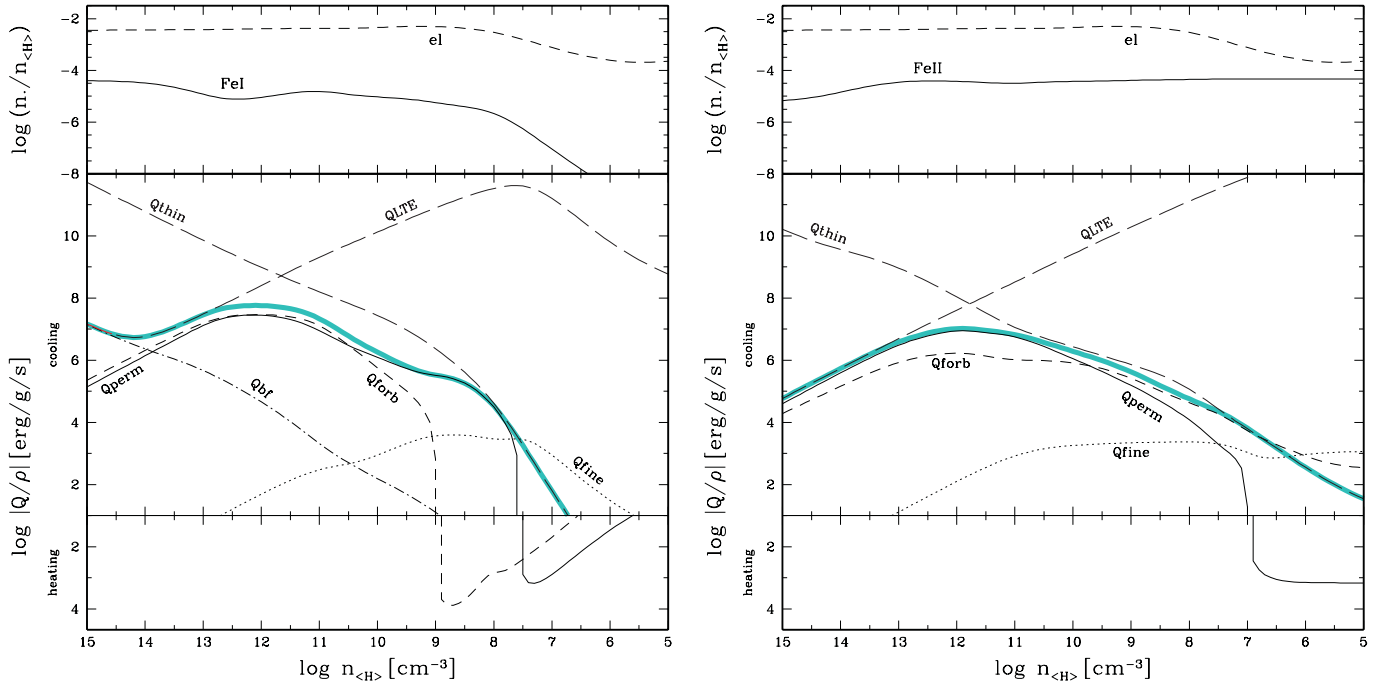


Fig. 7. Comparison to the results obtained in the LTE limiting case Q_{LTE} (including optical depth effects) and in the non-LTE optically thin case Q_{thin} . *Left hand side:* Fe I. *Right hand side:* Fe II. The *upper* diagrams shows the concentrations with respect to hydrogen. The thick full grey lines in the *lower* diagrams indicate the heating/cooling rates Q from the full non-LTE calculations including optical depths effects. Contributions by permitted, forbidden, fine-structure and bound-free transitions to this rate are also shown. Note the two-fold logarithmic scaling of the y -axis for heating and cooling as indicated. Fixed parameters are $T = 7000$ K, $T_{rad} = 3000$ K, $r/R_* = 2$ and $\langle dv/dl \rangle = 1$ km s $^{-1}$ /50 R_\odot .

Fig. 7 shows the results as function of density for a particular choice of temperature, radiation field and velocity gradient. In this case, the LTE-assumption yields approximately the same heating/cooling rate like the full non-LTE calculations at large densities $\log n_{(H)} \gtrsim 12.5$ (corresponding to $\log n_e \gtrsim 10$) concerning both Fe I and Fe II. Good agreement with the results in the optically thin limit are achieved for low densities $\log n_{(H)} \lesssim 8$ (Fe I) and $\log n_{(H)} \lesssim 10.5$ (Fe II), respectively. It is difficult, however, to generalise these findings to other conditions or other species, although the LTE-assumption seems to work reasonably fine for electron densities $\log n_e \gtrsim 9 \dots 11$. If the velocity gradient is increased by a factor of a 100, this “critical” electron density increases by a factor of about 10.

It is absolutely necessary to account for the optical depths effects in the lines. Ignoring these effects in the non-LTE case leads to an overestimation of the cooling rates by up to 5 orders of magnitude (see Figs. 7 and 9). When applying the LTE approximation and ignoring the optical depths effects (i. e. if both LTE and $P^e = 1$ is assumed)⁸, the deviations are even larger as a roughly constant value of $(Q_{thin LTE}(Fe I) + Q(Fe II))/\rho = -(2 \dots 6) \times 10^{13}$ erg g $^{-1}$ s $^{-1}$ is found in this case. These results cannot even be depicted in Fig. 7.

Fig. 7 also shows the individual contributions of bound-free transitions and permitted, forbidden and fine-structure lines. Note that for large densities, the bound-free transitions of Fe I actually dominate, whereas for medium densities, forbidden and

permitted lines are more important concerning both Fe I and Fe II. At low densities, fine-structure (and forbidden) lines cool the gas at the same time as permitted lines heat it, which indicates that the upper levels of the cooling transitions are radiatively pumped by the permitted lines.

5.4. Which lines are important?

Fig. 8 indicates where in the $(T, n_{(H)})$ -plane the different types of radiative transitions contribute most to the heating and cooling by Fe I and Fe II, depending on the background radiation field. In the case $T_{rad} = 0$, heating cannot occur and, consequently, the upper panels for heating are empty in Fig. 8. Considering trajectories of roughly decreasing temperature and density through the plane, we find in this case a certain sequence of the most important cooling process: bound-free – permitted – forbidden – fine-structure. In cases where a background radiation field is included, the results are more complex and the permitted lines seem to gain ground especially as heating agents. However, at small densities, the energy absorbed by the atoms in permitted and even in forbidden lines is partly re-emitted in other lines, usually at longer wavelength. Therefore, heating and cooling is important at the same time. Analysis of the rates in such cases reveal rich fluorescent pumping effects, e. g. the upper levels of fine-structure transitions are pumped by absorption in a permitted line followed by re-emission in another line of the same multiplet.

⁸ Equivalent to the usage of Planck means in Eq. (24).

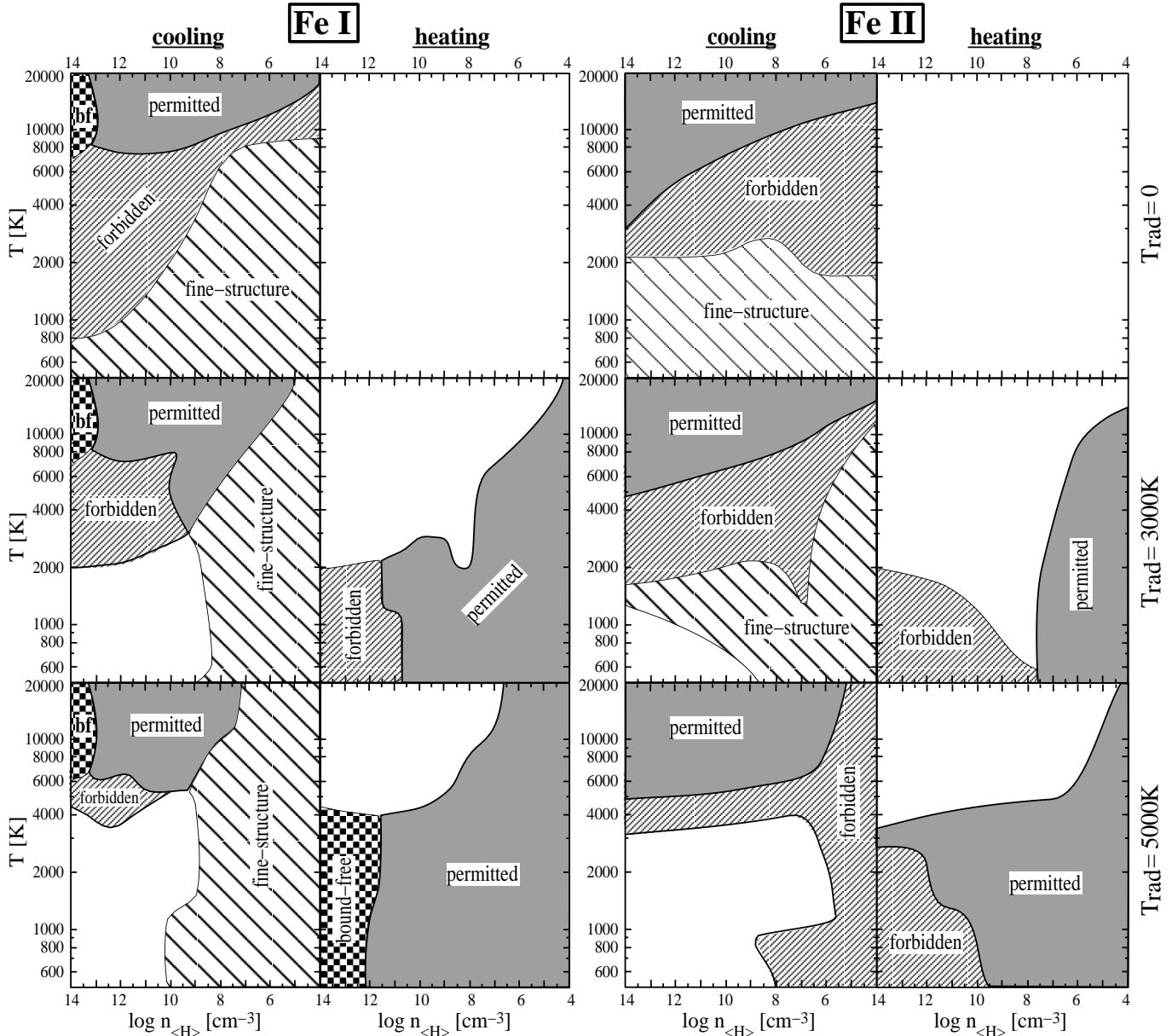


Fig. 8. Sites in the $(n_{\langle H \rangle}, T)$ -plane where the indicated type of radiative transition dominates the cooling (r.h.s.) and the heating (l.h.s.) by iron. Left column: Fe I — right column: Fe II. Blank regions indicate that none of the radiative processes is important for cooling or heating, respectively. The parameter T_{rad} is varied from zero (upper row) to 5000 K (lower row). Fixed parameters are $r/R_* = 2$ and $\langle \frac{dv}{dt} \rangle = 1 \text{ km s}^{-1}/50 R_{\odot}$.

5.5. Influence of the velocity gradient

The influence of the velocity gradient $\langle \frac{dv}{dt} \rangle$ on the results for the total cooling rate is demonstrated for Fe I in Fig. 9. At large densities, the cooling rates caused by line emission are strongly affected by self-absorption in the lines, which efficiently blocks the photons. At large Sobolev optical depth τ^S , this blocking reduces the cooling rates linearly with increasing density (see Eq. 6), since the escape probability scales as $P_{ul}^e \rightarrow 1/\tau_{ul}^S$ and $\tau^S \propto \rho$. The figure indicates that this blocking is already relevant at $\log n_{\langle H \rangle} \approx 8 \dots 9$, although the full effect develops at larger densities. This suggests that the cooling at medium densities is a superposition of optically thin and optically thick lines. At large

densities, all the relevant lines become optically thick, and the blocking acts at full strength.

5.6. Results as a function of the size of the model atoms

Fig. 10 shows the cooling rates of Fe II as function of the size N of the model atom. If only very few levels are included ($N = 2 \dots 5$), the model atom actually comprises only (parts of) the ground state quintet a^6D and, consequently, only accounts for fine-structure cooling. As the number of levels is increased, first the forbidden lines come into play, which are most effective for the chosen parameters in this plot. At $N = 36$, the first permitted lines enter into competition. However, these are

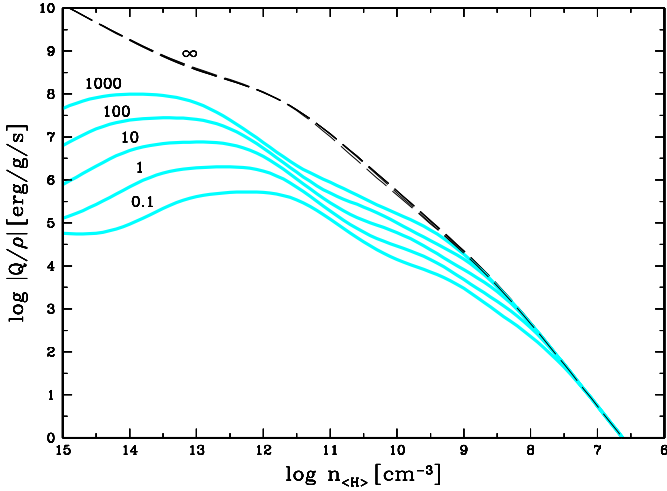


Fig. 9. Influence of the velocity gradient on the total cooling rate of Fe I. The labels indicate $\langle \frac{dv}{dt} \rangle$ in units of $\text{km s}^{-1}/50 R_{\odot}$. The $\langle \frac{dv}{dt} \rangle = \infty$ –curves are calculated by assuming $P^e = 1$ in each case (see Sect. 5.3). Other parameters are $T = 5000 \text{ K}$, $T_{\text{rad}} = 3000 \text{ K}$ and $r/R_* = 2$.

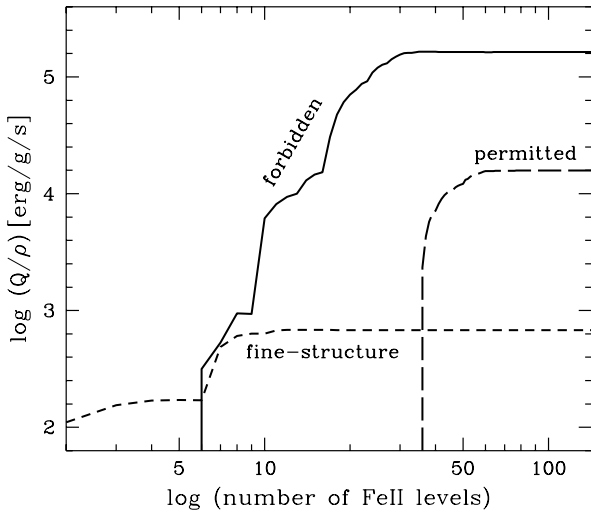


Fig. 10. Contributions of permitted, forbidden and fine-structure lines to the total Fe II cooling rate Q as function of the number of included levels N of the Fe II model atom. Parameters for this plot are $T = 5000 \text{ K}$, $n_{\langle \text{H} \rangle} = 10^{11} \text{ cm}^{-3}$, $T_{\text{rad}} = 3000 \text{ K}$, $r/R_* = 2$ and $\langle \frac{dv}{dt} \rangle = 1 \text{ km s}^{-1}/50 R_{\odot}$.

not as important as the forbidden lines. A further increase of N beyond a value of about 60 does not lead to any significant changes in the cooling rates, although the total number of lines still increases about quadratically with increasing N . We note that the energy of the 60th level $E_{60} \approx 14 \cdot kT$, which may serve as a rough guide on how much levels are to be included for a proper calculation of Q . However, the convergence of the results as a function of N depends on the relative importance on the different contributions of fine-structure, forbidden and permitted lines, and therefore depends on the physical conditions (see Fig. 8). For instance, if the permitted lines are most important (e. g. at high temperatures), more levels have to be included to reach convergence.

6. Discussion: why are the forbidden and fine-structure lines so important?

It seems to be a paradox: the permitted lines typically have radiative transition probabilities 4 ... 10 orders of magnitudes larger than the forbidden and fine-structure lines, but do not dominate the radiative heating and cooling according to the results of this paper⁹.

In the following, we will briefly discuss the radiative cooling by spectral lines in two important limiting cases. We neglect bound-free transitions, which enables us to evaluate the bound-bound radiative heating/cooling rate either from Eq. (6) or, alternatively, from Eq. (12):

$$Q^{\text{bb}} = Q_{\text{rad}}^{\text{bb}} = Q_{\text{coll}}^{\text{bb}} \quad (25)$$

1) Cooling in the low-density limit: When the density of the gas is very small, the upper levels mostly de-populate radiatively, because the radiative lifetimes are much shorter than the characteristic time-scales for collisional de-excitation ($A_{ul} \gg C_{ul}$)¹⁰. Consequently, the upper levels are much less populated with respect to LTE: $n_u \ll n_{\ell} \frac{g_u}{g_{\ell}} \exp(-\frac{\Delta E_{u\ell}}{kT})$. This relation can be used straightforwardly in Eq. (12), so we choose to calculate $Q_{\text{coll}}^{\text{bb}}$. The condition that the upper levels are less populated than in LTE also implies that the collisional excitation occurs mainly from the ground level, i. e. we can approximately truncate the first sum in Eq. (12) after $\ell = 1$. Furthermore, for simplicity, we put $n_1 \approx n_{\text{tot}}$ and roughly assume that the collisional de-excitation rates (electron collisions only) $C_{u1} = n_e \gamma_{u1}^e$, which are in fact slowly varying temperature-functions, are given by a universal constant $\Gamma = \gamma_{u1}^e g_u / g_1$. Eq. (12) then becomes

$$Q^{\text{bb}} \approx -\Gamma \cdot n_e n_{\text{tot}} \cdot \sum_{u=2}^N E_u e^{-\frac{E_u}{kT}} \quad (26)$$

Eq. (26) states that the cooling rates of spectral lines are not at all dependent on the number or the properties of the lines but do only depend on the collisional properties of its carrier in this case¹¹. Since the function $x \exp(-x/kT)$ has its relative maximum at $x = kT$, we conclude that in the low-density limiting case

- the cooling rates linearly depend on $n_e n_{\text{tot}}$ (roughly $\propto \rho^2$), favouring abundant elements (e. g. C, N, O),
- most important contributions come from those *upper levels* u which have $E_u \approx kT$ (implying $h\nu \lesssim kT$). Therefore, the most efficient cooling lines are expected to be low-excitation lines in the infrared (e. g. at $\lambda \gtrsim 2.9 \mu\text{m}$ for $T = 5000 \text{ K}$).

⁹ The terms “important” and “dominant” in this context concern the net local energy exchange between the gas and the radiation field, which is different from being important in radiative transfer or for the emergent spectrum.

¹⁰ This is the typical “nebular” case (e. g. Osterbrock 1974)

¹¹ Supposed that some lines are present which are capable of driving the N -level system into the discussed case.

2) *Cooling in the optically thick LTE case:* When the gas is hot and dense enough to keep the level populations close to LTE, we use Eq. (6). The escape probabilities in the optically thick limit in Sobolev-approximation are given by $P_{ul}^e \rightarrow 1/\tau_{ul}^S = 8\pi\nu_{ul}^3(c^3 A_{ul})^{-1} \langle \frac{dv}{dl} \rangle (n_l g_u / g_l - n_u)^{-1}$. We neglect stimulated emission ($n_l g_u / g_l \gg n_u$) and put $j_{\nu_{ul}} = 0$ as we are interested in cooling and not in heating. Furthermore, we apply the Boltzmann distribution $(g_l n_u) / (g_u n_l) = \exp(-\Delta E_{ul} / kT)$. Eq. (6) then becomes

$$Q^{\text{bb}} \approx - \left\langle \frac{dv}{dl} \right\rangle \frac{8\pi}{h^3 c^3} \sum_{\text{lines}} \Delta E_{ul}^4 e^{-\frac{\Delta E_{ul}}{kT}}. \quad (27)$$

Eq. (27) states that the line-cooling does not depend on the density of the carrier, nor on the “strength” of the lines (the Einstein coefficients A_{ul})¹². Since the function $x^4 \exp(-x/kT)$ has its relative maximum at $x = 4kT$, we conclude that in the optically thick LTE limiting case

- the cooling rates depend linearly on $\langle \frac{dv}{dl} \rangle$,
- the cooling rates are roughly density-independent, which means that the cooling rate per mass decreases linearly with increasing density (hence, trace elements may be as important as abundant elements),
- the cooling rates depend linearly on the *number of lines* in the spectral region $h\nu \approx 4kT$. The most efficient cooling lines in this case are therefore expected to lie in the optical spectral region (e. g. at $\lambda \approx 720$ nm for $T = 5000$ K).

In both considered limiting cases, the radiative cooling by spectral lines does not depend on the strength of the lines, e. g. permitted lines are in fact not favoured. In contrast, the other listed criteria (i. e. the number of lines in case 2 and especially the low excitation energy in case 1) in fact suggest that forbidden and fine-structure lines are more important in both limiting cases.

7. Conclusions

The radiative heating and cooling rates of Fe I and Fe II have been calculated under various temperature, density and radiation field conditions typical for the extended atmospheres and circumstellar envelopes of cool stars. The calculations are based on large non-LTE model atoms, include a few thousands of fine-structure, forbidden, permitted and bound-free transitions, and rely on statistical equilibrium in the Sobolev limit.

In comparison to other heating/cooling agents, Fe I and Fe II have been found to be important especially at medium temperatures ($T \approx 3000 \dots 9000$ K) between the molecular domain and temperatures appropriate for the effective collisional excitation of the hydrogen atom. The high efficiency of iron is caused by its numerous low-excitation states in combination with its large number of spectral lines, which can easily outweigh the fairly small abundance of this element in comparison to others, e. g. C, N, O.

The calculation of the line-cooling rates requires both a non-LTE treatment of the problem (especially at small densities) and

a treatment of the optical depth effects in the lines (especially at large densities). Simple formulae for the line-cooling, like $\rho^2 f(T)$ or the application of mean LTE-opacities, just fail for those densities ($\sim 10^9 \dots 10^{12} \text{cm}^{-3}$), where the formation of chromospheres, the dust formation, and the driving of stellar winds is expected to occur.

A lot of the cooling by iron in fact involves fine-structure, forbidden and semi-permitted lines, as the strong permitted lines are also strongly blocked. The numerical results as well as the general considerations in Sect. 6 suggest that infrared low-excitation lines with ($E_u \approx kT$) work best at small densities, whereas the total number of lines with ($h\nu \approx 4kT$) is important at large densities.

For grey LTE hydrodynamical models we cannot recommend the use of Planck means in the energy equation, as this approximation ignores the blocking of the emitted line photons completely, which leads to cooling rates being too large by 5 orders of magnitude or more. Rosseland means (scattering-free), which essentially account only for the continuum heating/cooling, are apparently the better choice in grey LTE models. However, as the assumption of LTE does not hold in stellar winds, also the application of Rosseland mean opacities is questionable. The non-LTE heating/cooling rates per mass strongly decrease with decreasing density and this behavior is usually not revealed when Rosseland means are applied. Furthermore, line cooling is definitely more important at small densities ($n_{\text{H}} \lesssim 10^{13} \text{cm}^{-3}$).

The calculated radiative cooling rates of iron are found to be larger in general, less temperature-dependent and less density-dependent than what is usually assumed in hydrodynamical models using pre-calculated non-LTE cooling laws (e. g. Bowen 1988, Cuntz 1990). These findings may provide new clues to chromospheric heating mechanisms and to the propagation of shock waves in the envelopes of cool stars. The radiative cooling time-scales of the gas due to iron alone are found to be much shorter as compared to these models in the important temperature-regime $T \approx 3000 \dots 9000$ K. Furthermore, the results of his paper may shed some new light on the driving of cool star winds by pulsation, since the overall efficiency of radiative heating/cooling can have a dramatic influence on the results of model calculations concerning this driving mechanism (Willson & Bowen 1998). The present results for iron cooling suggest a larger heating/cooling efficiency of the gas, possibly leading to smaller pulsation-driven mass loss rates.

The ionisation balance in the envelopes of AGB stars is strongly controlled by photospheric (+chromospheric) radiation. The present calculations indicate that the Fe II/Fe I-ratio is mainly a function of density and (UV) radiation field rather than a function of temperature, which favours large degrees of ionisation at small densities. This might partially explain the detection of both unexpectedly strong Fe I and Fe II fine-structure lines in M-type and C-type giants (Aoki et al. 1998). Depending on the conditions, the fine-structure lines can be strongly pumped by fluorescence which may cause excitation temperatures of several thousand degrees above the thermal level. Thus, the present paper suggests the emergence of much larger fluxes

¹² As long as the density of the carrier and the Einstein-coefficients of the lines assure optical thickness in the lines.

in the fine-structure lines as compared to predictions based on LTE.

Acknowledgements. The topic of this paper has been seeded by fruitful discussions with Prof. Dr. L. A. Willson. We would like to thank Christiane Helling, Dr. Andrej Fokin and Prof. Dr. P. Cottrell for their valuable comments on the manuscript and the hospitality of the Department of Physics and Astronomy at the University of Canterbury, New Zealand, where this paper was completed. This work was supported by the German *Deutsche Forschungsgemeinschaft*, DFG project number Se 420/15–1.

References

- Allen C.W., 1973, *Astrophysical Quantities*. The Athlone Press, London
- Anders E., Grevesse N., 1989, *Geochimica et Cosmochimica Acta* 53, 197
- Aoki W., Tsuji T., Ohnaka K., 1998, *A&A* 333, L19
- Bowen G.H., 1988, *ApJ* 329, 299
- Burgess A., Tully J.A., 1992, *A&A* 254, 436
- Carpenter K.G., Robinson R.D., Johnson H.R., et al., 1997, *ApJ* 486, 457
- Cuntz M., 1990, *ApJ* 349, 114
- Dere K.P., Landi E., Mason H.E., Monsignori Fossi B.C., Young P.R., 1997, *A&AS* 125, 149
- Drawin H.W., 1969, *Zs. Phys.* 225, 483
- Fleischer A.J., Gauger A., Sedlmayr E., 1992, *A&A* 266, 321
- Fokin A.B., 1992, *MNRAS* 256, 26
- Fuhr J.R., Martin G.A., Wiese W.L., 1988, *J. Phys. Chem. Ref. Data* 17, Suppl. 4
- Gauger A., Fleischer A.J., Winters J.M., Sedlmayr E., 1993, *AG Abstr. Ser.* 9, 127
- Höfner S., Jørgensen U.G., Loidl R., Aringer B., 1998, *A&A* 340, 497
- Hollenbach D., McKee F., 1989, *ApJ* 342, 306
- Kurucz R. L., 1988, In: McNally M. (ed.) *Transactions of the International Astronomical Union XXB*. Kluwer Academic Publishers, Dordrecht, p. 168
- Landini M., Monsignori Fossi B.C., 1990, *A&AS* 82, 229
- Linsky J.L., Harper G.M., Bennett P.D., Brown A., Valenti J., 1998, In: Kaper L., Fullerton A.W. (eds.) *Cyclical variability in stellar winds*. Springer, p. 294
- Luttermoser D.G., Johnson H.R., 1992, *ApJ* 388, 579
- Mendoza C., 1983, In: Flower D.R. (ed.) *Planetary Nebulae*. D. Reidel Publishing Company, Dordrecht, p. 154
- Osterbrock D.E., 1974, *Astrophysics of Gaseous Nebulae. A Series of Books in Astronomy and Astrophysics*. W.H. Freeman Company, San Francisco, 1. edition
- Seaton M.J., Yan Y., Mihalas D., Pradhan A.K., 1994, *MNRAS* 266, 805
- Vernazza J.E., Avrett E.H., Loeser R., 1981, *ApJS* 45, 635
- van Regemorter H., 1962, *ApJ* 136, 906
- Willson L.A., Bowen G.H., 1998, In: Kaper L., Fullerton A.W. (eds.) *Cyclical variability in stellar winds*. Springer, p. 294
- Woitke P., Krüger D., Sedlmayr E., 1996, *A&A* 311, 927